Towards a 3g Crawling Robot through the Integration of Microrobot Technologies*

Ranjana Sahai, Srinath Avadhanula, Richard Groff, Erik Steltz, Robert Wood, and Ronald S. Fearing

Electrical Engineering and Computer Science Department
University of California, Berkeley
Berkeley, CA 94720 USA

rsahai@eecs.berkeley.edu or ronf@eecs.berkeley.edu

***Abstract* - This paper discusses the biomimetic design and assembly of a 3g self-contained crawling robot fabricated through the integrated use of various microrobot technologies. The hexapod structure is designed to move in an alternating tripod gait driven by two piezoelectric actuators connected by sliding plates to two sets of three legs. We present results of both the kinematic and static analyses of the driving mechanism that essentially consists of three slider cranks in series. This analysis confirmed the force differential needed to propel the device. We then review various other microrobot technologies that have been developed including actuator design and fabrication, power and control electronics design, programming via a finite state machine, and the development of bioinspired fiber arrays. These technologies were then successfully integrated into the device. The robot is now functioning and we have already fabricated three iterations of the proposed device. We hope with further design iterations to produce a fully operational model in the near future.**

Index Terms – biomimetics, crawling microrobots, design and fabrication

I. Introduction

Currently in robotics, biomimetics and miniaturization are two common trends. From minimally invasive surgery instruments that are inspired by tapeworms [1] to miniature aircraft inspired by flies [2], scientists continue their quest to make even smaller robotic devices and, while doing so, increasingly look to nature for guidance. Unfortunately, designing and manufacturing these tiny structures are often limited by processes that are expensive and not easily accessible.

Thus, the motivation behind the work presented here is the need to have suitable methods for easily prototyping such devices. In our chosen area of concentration, the centimeter and sub-centimeter-sized scale, we are looking to develop and integrate technologies that would allow this easy prototyping. Our ultimate goal will be to reduce these processes into a kit of components from which a variety of such prototype structures can be made in a relatively low cost fashion.

As a step in this direction, this paper looks at combining various structure fabrication processes, actuators, and power electronics developed particularly for structures of this size in our own chosen biomimetic robot design, a 3g crawling robot. We discuss the design and assembly of this device, provide brief descriptions of the various integrated technologies, and, finally, give our results and conclusions from following this process.

II. Robot Design

A. Background

The development of a robot with legs as opposed to wheels (nature's solution for adapting to various types of terrain) has been investigated as far back as 1940. Reference [3] provides a review of some of these various designs over the years. Some other designs of particular note from the point of view of biomimetic structures and terrain adaptability include Stanford's SpinybotII (uses lessons learned from insect spines to design a robot capable of climbing various rough surfaces [4]), University of Michigan's RHex (takes advantage of compliant legs that make a full rotation to achieve high terrain adaptability with no sensing [5]), and the hybrid leg and wheel motion of Case Western's Mini-Whegs [6]. In terms of size, however, the robot we are building here more closely resembles efforts such as in [7] and [8] although our structure is larger than both these cases. Table 1 summarizes the features of our design with other legged or wheeled mechanisms on this scale.

TABLE I
Comparison of Various Microrobots

Robot	Mass	Velocity	Size	Tethered	Motion
Sandia's	28g	8.5 mm/s	6.35 mm	No	Wheeled
Hollar's Solar Powered Ant	10.2 mg	1.3 mm/s (design)	8.6mm	No	Not yet
Ebefors	83 mg	6 mm/s	15mm	Yes	Legged
EPFL's Inchy	Not listed	30 cm/s	25 mm	No	Wheeled
Our design	3.1g	10 mm/s (design)	35mm	No	Not yet

We should also note that from the two basic types of robotic structures, serial or parallel, we are focusing on flexure-based parallel mechanisms. Serial mechanisms have an open kinematic structure and are simple to design. However, several of their joints have to be actuated either through joint based actuators or through cables operated by ground-based motors. This limits their performance,

* This work has been supported by the following grants: NSF DMI-0423153 and NSF DMI-0115091.

dynamics and positioning accuracy. Parallel mechanisms based on closed kinematic chains, on the other hand, are free from these limitations since they can be operated by using only ground-based actuators. Since all the joints except the ground ones are passive, it is relatively simple to incorporate flexure joints in parallel mechanisms. This is desirable from our standpoint since flexure joints are easier to manufacture on the centimeter-size scale.

B. Basic Structure

The basic structure chosen for our particular crawler is shown in Fig. 1. Each leg is the familiar slider crank where the crank is extended to form the leg as shown. Further details of the leg mechanism are provided in a later section. To simplify the structure and reduce the number of actuators required, the six legs are broken into two sets of three coupled motions through the use of two linear slides. This produces a tripod gate as will be discussed in a later section. Finally, there is another four-bar structure to transfer the actuator motion to each of the slides.

The three mechanisms (the leg, the slide, and the connection to the actuator) are basically just a series of three slider crank mechanisms. The kinematics of slider cranks has been worked out in several sources, such as in [9], so we shall not repeat the derivation here. Fig. 2, however, presents the results of such a kinematic analysis applied to the combined structure. It shows the motion the various components go through and the arc subtended by the foot. Fig. 3 shows the displacements of the actuator, the slide, and the foot (horizontal component) during this simulated motion. One can clearly see the magnification that occurs over the various stages.

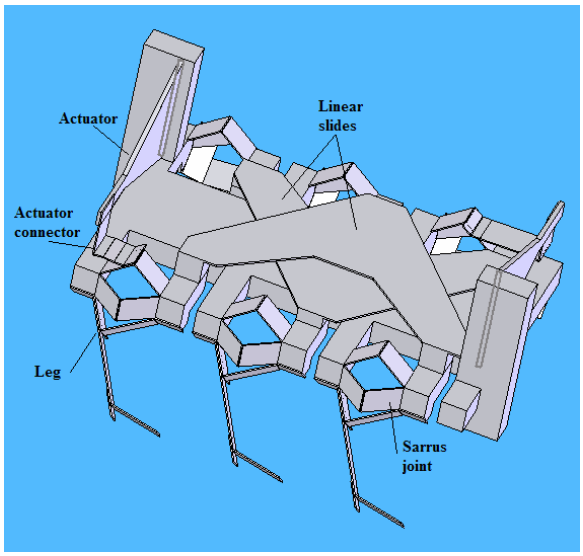

Fig. 1 SolidWorks® Conception of the Mechanical Structure of the Crawler (The board and battery are not shown.)

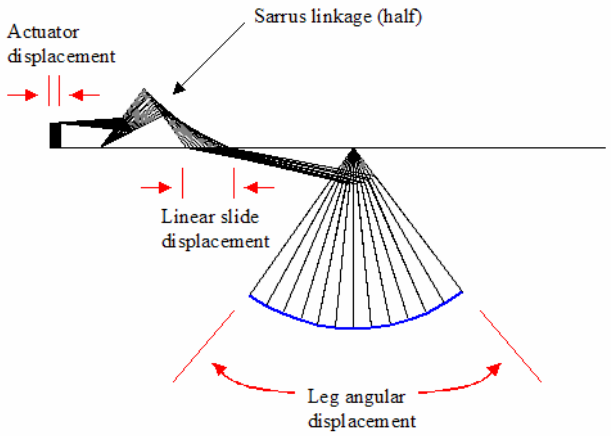

Fig. 2 Motion of the Leg Driving Mechanism

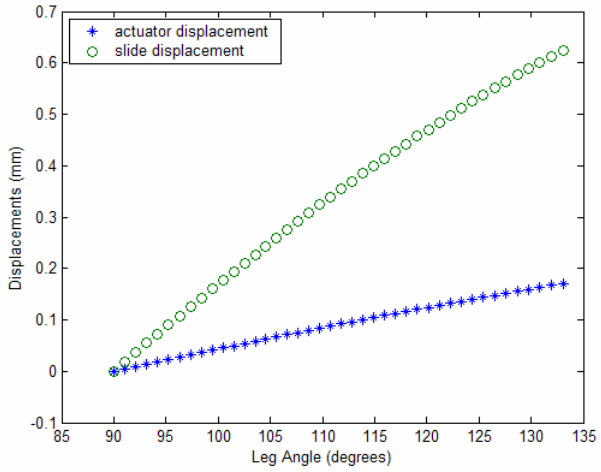

Fig. 3 Displacements of the Actuator and Slide

C. Linear Slides using Sarrus Linkages

Sliding motion is actually challenging to achieve using just simple flexures. Reference [10] lists a few methods of achieving exact straight-line motion with such mechanisms. Of these, the one of most interest to us was the non-planar Sarrus linkage. Despite the 2D nature of the linkage, it seemed to be the simplest method for achieving the needed limited linear motion in our structure. The linkages are used to connect each of the sliding portions of the leg mechanism to the central body of the crawler, and then a plate is used to tie three of the legs' motion together. The result is essentially a sliding plate that is connected to the central body at three points through Sarrus linkages.

D. Differential Foot Mechanism Force Analysis

A common and popular technique for the analysis and design of compliant mechanisms is the pseudo rigid body method (PRBM) [9]. In this lumped approach, appropriately positioned pin joints with torsional springs to represent the non-zero stiffness of the flexures are used in place of the flexural joints. This results in an equivalent rigid body system that can be analyzed by relatively simple standard procedures.

Since the crawler is expected to undergo only slow motion, a quasi-static analysis is adequate. Even with this assumption, an exact analysis will be quite complicated because of the presence of several flexure elements that undergo large nonlinear deflection. However, it has been amply demonstrated that, in the case of slider crank mechanisms, the PRBM analysis yields fairly accurate results (within 2% of nonlinear finite element analysis results) [9]. We will use the PRBM for this preliminary design study. We will further assume that the flexure lengths are small compared to the link lengths. The equivalent torque is given by $T = k\,\psi$ where k is the stiffness and ψ is the relative change in the joint angle from the initial configuration. The stiffness is $k=EI/L$ where E is the modulus of elasticity, I is the cross-sectional moment of inertia, and L is the length of the flexure. It should be noted that this represents the stiffness of the equivalent torsional spring and not that of the original flexural beam. Once the flexures are replaced by torsional springs, the equivalent mechanism contains only rigid links connected by pin joints thus making the analysis much easier.

The equations governing the statics of a flexure jointed slider crank mechanism are well known (see [9], for example). Using the slider crank as a building block, we have carried out the equilibrium analysis of the entire structure. For this study, however, we will present the results of a PRBM analysis applied to the leg structure alone, a simple slider crank where the leg is formed by extending the crank. Since the leg has only one degree of freedom, towards the end of the leg we have added an additional flexure with a mechanical stop on one side (see Figure 1). This allows us to create a differential force that should allow forward motion.

We will consider impending motion in two directions. In one case the mechanical stop is operational and the entire leg acts as a single rigid body, and in the other the flexural spine allows the bottom portion to bend. Once the PRBM model has been created, the static analysis can be carried out by considering the free-body diagrams of the member links. The PRBM analysis of a generic slider crank mechanism in [9] applies directly to the leg mechanism here. In the case in which the flexural spline is active, we need to consider an additional free body diagram of the bottom element. By assuming that a single leg bears the entire weight of the structure (taken as 4g to allow for a safety factor), the horizontal component of the foot reaction can be calculated for a given force exerted on the driving slider. It is noteworthy that impending motion occurs when the horizontal component reaches a value of μ (coefficient of friction) times the vertical component. The results presented in Fig. 4 clearly show the horizontal force differential between the non-flexing and flexing knee cases that is required for movement as stated earlier. The forces shown have been normalized by dividing by the force on the slide. It is noteworthy that the maximum force differential occurs when the leg angle equals approximately 75°

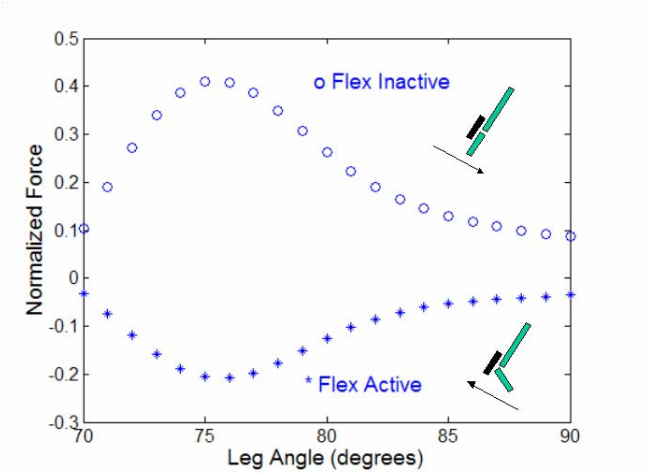

Fig 4 Difference in Normalized Force (depending on whether the flexure in the leg is allowed to flex or not)

III. Manufacture and Assembly of the Crawler

A. *Central Body*

We used a three step molding process to fabricate the body of our crawling mechanism as shown in Fig. 5. First, the body was fabricated in wax from a SolidWorks® model using a 3D wax printer (ThermoJet printer from 3D Systems). A negative of the wax model was then cast in silicone rubber. Finally, the rubber mold was used to create the final polyurethane part. In later models, we used this casting process to our advantage by embedding the battery in the structure of the polyurethane body itself. This allowed us to make a more streamlined structure whose center of gravity was closer to the ground. The rubber mold also served a secondary purpose as an alignment fixture that held the various body parts in place while the Sarrus linkages and linear slides were being assembled.

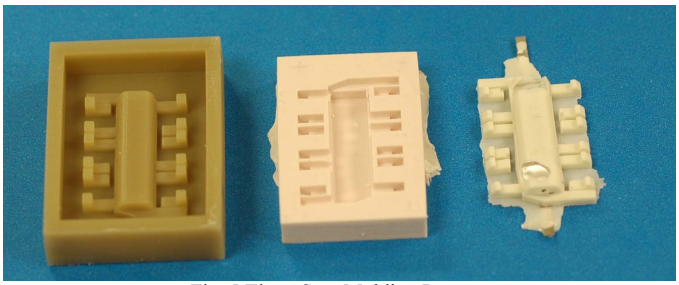

Fig. 5 Three Step Molding Process
(From left to right - wax mold, rubber mold, and polyurethane part with a battery embedded in it.)

B. *Sarrus Linkages and the Linear Slides*

All parts involving flexure joints were fabricated from 12µm polyester sheets (flexure material) sandwiched between two layers of carbon fiber (link material) similar to the techniques developed in [11]. These parts are first cut out (using a laser) in a 2D plane and then folded and glued in their final 3D configuration (see Fig. 6). As mentioned in [10], it is important for the Sarrus linkages to be fabricated with a 90°

bend or binding in the linkage motion may occur. This is avoided by using the polyurethane body as a guide, which was molded to have exact 90° angles. Gluing all the parts together in the rubber mold and using its edges as a guide also achieved the necessary alignment of the six different Sarrus linkages that make up the structure.

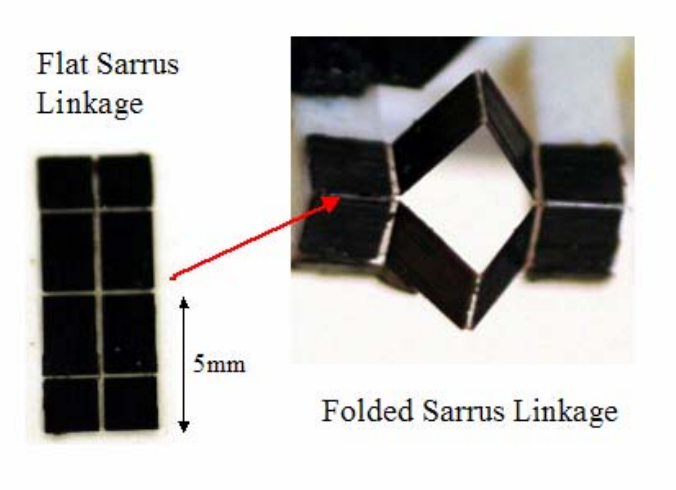

Fig. 6 Flat and Fully Assembled Sarrus Linkage

C. *Leg Mechanism*

The legs were also manufactured using the same technique as the Sarrus linkage (polyester sandwiched between two layers of carbon fiber). A flattened version of the leg is shown in Fig. 7 followed by how it looks when the leg is folded. This folded structure is then attached to the robot's body with the sliding plates. The final structure (including the addition of integrated microrobot technologies described below) is shown in Fig 8.

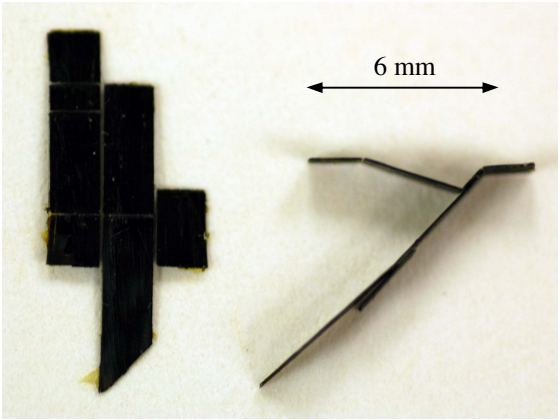

Fig. 7 Flat and Fully Assembled Slider Crank Leg

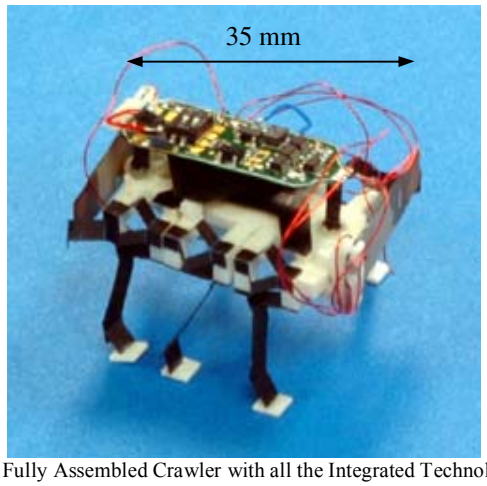

Fig 8 Fully Assembled Crawler with all the Integrated Technologies

IV. Integrated Technologies

Given the design and construction of the mechanical structure of the robot, it still requires the addition of some type of actuator, power source (or battery), power and control electronics, and some sort of rudimentary programming in order for it to move. Below we discuss each of these technologies. Although they were developed for other applications, we hope to be able to adapt and integrate them onto our structure.

A. *Actuator Design, Construction and Performance*

There are several types of actuators that could have been used for the crawler. However, because of convenience and the reciprocating nature of the leg motions, piezoelectric bimorph actuators were chosen, specifically, clamped-free bending cantilevers. Such actuators are easily incorporated into the structure and have moderate force and displacement characteristics compared to other bending actuator morphologies. The only drawback with these actuators is the necessity of high voltage source and drive electronics (see the following subsection).

The design of the actuators is similar to the energy density optimization described in [12]. Given certain geometric constraints, the length, width, extension ratio, and width ratio are all determined based upon the laminate plate design presented in [12] as well as the number and orientation of the constituent layers. After these parameters are chosen, the individual laminae are laser micromachined, layered (as is shown in Fig. 9), cured, and released. The current actuators have a total length of 20mm, a width of 7mm, extension and width ratios of 0.25 and 1.15 respectively, and a single carbon fiber central layer with a thickness of 40μm. Once the actuators are released they are embedded in a short-fiber-composite reinforced polymer base and the electrodes are wired. These actuators exhibit a displacement of 1.2mm and a blocked force of 450mN.

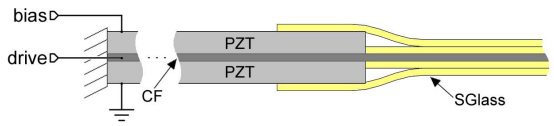

Fig. 9 Cross Section of the Crawler Bimorph

B. *Power and Control Electronics Design*

As mentioned above, the piezoelectric cantilever actuators used on this robot require high voltage (around 200V) to properly move the legs. Since we are using a 3.7 V battery, this means we need to significantly step up the drive voltage. We also need adequate ability to control the robot, which calls for some type of onboard processing.

Ideally, off the shelf or previously researched technology could be used for this purpose. Piezoelectric actuators have been used in autonomous microrobots before, most notably in the MICRON robot [13]. For this robot, a custom integrated circuit [14] was created to generate approximately 50 VDC for actuator drive. This is adequate voltage for low strain cantilever or stack piezoelectric actuators. However, for our high strain cantilever actuators, 50 VDC is not adequate. Therefore, we choose to go with the power and control board used in a microglider application as described in [15]. A picture of the power and control board appears in Figure 11. It provides approximately 200 VDC using a custom charge pump cascaded after a commercial boost converter, and has a 1 Mips processor onboard. The board is programmed using IR communications as is described in the following section, and has many other possible sensing features that can be added on, such as light seeking or optical flow sensing [15]. The board itself is made out of 50µm polyimide flex circuit, and populated weighs approximately 440 mg.

The battery chosen for the crawler is a 3.7V, 20mAh lithium polymer battery by Kokam. After the packaging and leads are trimmed, it weighs approximately 650mg. The battery can be discharged at up to 200mA, but for the crawler walking at a low frequency, the current draw is under 10mA, meaning it can operate for more than 2 hours. To our knowledge, this battery's power density of 114 J/kg at 1C is the highest that satisfies our weight constraints.

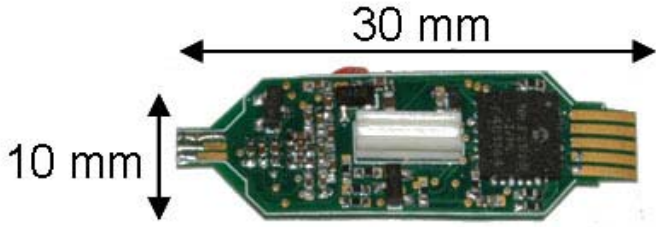

Fig. 10 Lightweight power and control electronics board

C. *PIC Programming via a Finite State Machine*

Traditionally, the PIC 2520 (the one used on our board) needs to be physically connected to a PC for re-programming. This is cumbersome, however, considering the delicate nature of the overall mechanism as well as the board. In order to reduce the risk of damage, a method to *wirelessly* re-program the behavior of the PIC was found. This method relies on the fact that most behaviors that we want the machine to exhibit can be expressed by a reasonably compact augmented FSM (finite state machine)[1]. Moreover, as reported in [16], state machines are extremely useful in controlling embedded systems because they allow us to maintain a clear seperation of the behavioral algorithms from the actual hardware implementation details.

In the present setup, the PIC 2520 is initially loaded with an *FSM emulation program* that can understand and model a (reasonably) arbitrary FSM. The state transition table is described on a host PC in simple XML format, which is then converted into a compact bit-stream representation. We connect an LED to the serial port of the host PC, so that when we write the bit-stream to the serial port in the RS-232 format, the LED flashes. These flashes are detected by an IR phototransistor connected to the A/D channel of the PIC. The A/D reading is thresholded and then converted back into the transmitted bit-stream. The bit-stream is then restructured into a FSM state table by the FSM emulation program in the PIC.

The FSM emulation program then steps through the FSM and exhibits the behavior specified therein. While stepping through the FSM, the program also monitors the phototransistor and if it receives a certain (improbable) sequence of values, it erases the current FSM and waits for a new FSM description. This way, we can reprogram wirelessly by flashing a pre-determined sequence of bits at the phototransistor.

The transition checking condition can utilize any of the following input peripherals:

- **A/D reading(s):** These are values read in over the A/D channels of the A/D. The FSM is thus necessarily independent of the exact sensor we place on the board. For the current revisions, we use two photo-transistors pointing in different directions.
- **Local timer:** This is the value of the number of FSM *ticks* elapsed since the last state transition.
- **Global timer:** This is the value of the number of FSM ticks since we first started stepping through the FSM.

In addition, while in each state, the FSM can assign any of the following output peripherals:

- **LED(s):** We are able to flash LED(s) at the tick frequency of the FSM which could conceivably allow us to set up a two way communication link using just the FSM. For now, we use the LED to simply provide visual cues about the present state of the FSM.
- **PWM(s):** This sets the duty-cycle of the two PWMs that are connected to the actuators.
- **Global timer:** We make the global timer re-settable to enable us to write nested looping behaviors.

[1] augmented in the sense that we also maintain a *timer* variable

In order to keep the program simple, we use the following simplified form for a transition checking condition:

```
IF (EXPRESSION) IS TRUE
       GOTO (transition_target)
ELSE
       STAY
```

where the grammar for the EXPRESSION is given as:

```
EXPRESSION := (LHS) (comparision_op) (RHS)
RHS := 16 bit number
    := input peripheral value
    := RHS (binary_op) RHS
LHS := RHS
comparision_op := >, <, ==
binary_op := +, -, /, *
```

The following example describes a behavior where the insect crawls straight for 10 seconds followed by a ``turn towards the stronger light" behavior using the above FSM framework:

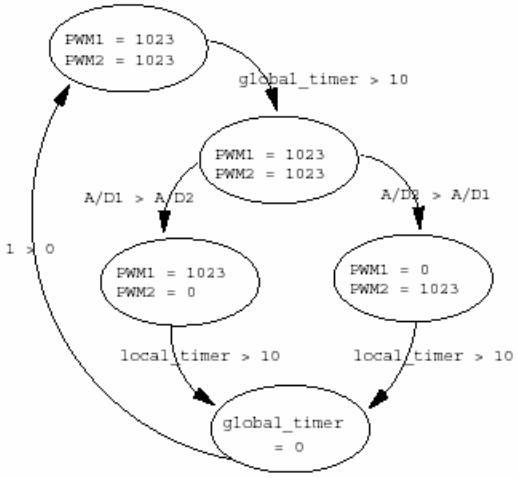

Fig. 11 FSM Example

In the above example, the insect crawls with equal stroke on both legs for 10 seconds and then decides to turn either right or left based on which A/D signal is stronger. Increasing the actuation on one of the tripods skews the gait and hence makes the insect move to one side.

D. Bioinspired Fiber Arrays for Directional Friction

Many species of animals have hair-, spine-, and bristle-like features used for the purpose of adhesion and directional friction. For example, geckos have arrays of spatula-tipped microhairs on their toes for adhesion [17], cockroaches have directional spines on their legs for support of misplaced feet on rough terrain [18], and earthworms have angled bristles that provide directional friction, i.e. greater shear force in one direction than in the opposite direction [19].

In [20], it was noted in the context of gecko-inspired adhesives that simple angled cantilevers can provide directional friction due to jamming. Shear forces can be developed when a fiber tip catches on a surface asperity and the friction cone contains the fiber's axis. If all fibers are angled similarly, then the array should also display directional friction. These angled arrays are similar in concept to the microspines used in [4], but at a smaller size scale.

Inspired by the biological examples, we manufactured fiber arrays for the feet of the crawler to serve as directional friction pads. First, we manufactured polyimide fibers, 2µm in diameter and 20µm long, using the process described in [21]. Then, a PDMS mold of these polyimide fibers was made. This mold is reusable and allows us to cast polyurethane and other polymers that are incompatible with the etching process described in [21]. Polyurethane is vacuum cast into the mold and allowed to cure. The fibers can be angled by peeling the pad out of the mold before curing is complete or by mechanically combing the fibers over. The current samples are not displaying the predicted directional friction, but by adjusting the geometry of the fibers (or alternatively, by selecting an appropriately structured surface) directional friction should be attainable.

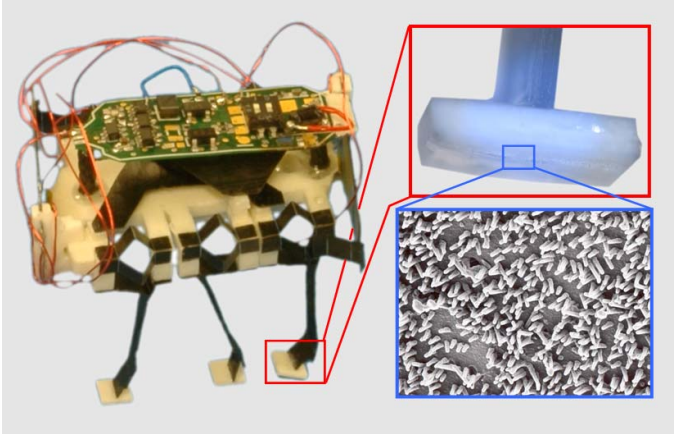

Fig. 12 Crawler's Feet
The crawler's feet are 3mm x 3mm squares of polyurethane. The fibers covering the bottom of the feet are 2µm in diameter and approximately 15µm long, and angled relative to the substrate by combing. Fibers with this geometry are too stiff to act as an adhesive, but should provide directional friction properties.

V. Results

We were able to combine the various technologies above successfully in at least three prototype crawling mechanisms to date. Fig. 13 shows these completed mechanisms. For the first iteration (the first robot on the left in Fig. 13), we focused on testing the mechanical mechanisms of the design by building the structure of the robot up to the point of attaching one actuator. This structure was then tested by suspending it in air and running the actuator wired to external power amplifiers for both the bias and drive voltages. With a bias voltage of 200V and a 1Hz, 120V amplitude drive voltage, the resulting leg stroke was measured to be around 40° with a corresponding linear slide movement of around 640µm.

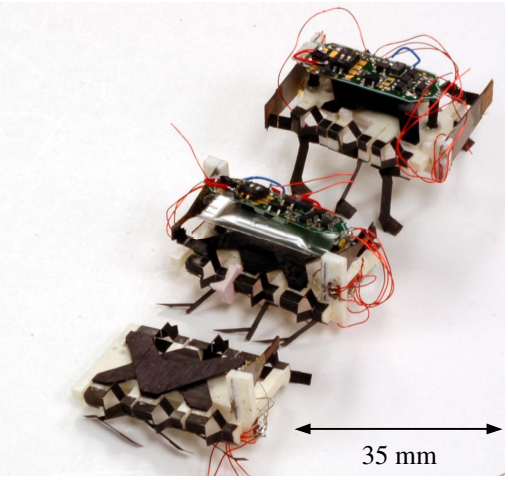

Fig. 13 Three Prototype Crawling Mechanisms

For the second iteration, both actuators were attached and the power and control electronics along with the battery were also integrated onto the structure (the middle robot in Fig. 13). Before integrating the board on the robot structure, the FSM emulation program was loaded into the PIC. While the robot was suspended in air, we were able to actuate both sets of leg. The PIC could also be successfully reprogrammed so that the two sets of legs could be programmed to actuate in sequence with each other and out of it. Unfortunately, issues with the construction of this robot – some slightly misaligned parts, glue in the flexure joints, and issues with how the actuators were attached to the structure – led to poor resulting motion in the legs. Although the structure was placed on the ground and allowed to run, it did not crawl. This mostly seemed due to the poor leg stroke and the fact that the give in the flexure joints allowed for motion up and down in the linear slides rather than lifting the structure.

The third iteration (shown on the right in Fig. 13) corrects some of the problems seen in the second iteration. The body was modified to give symmetry in the connection of the actuators. Also, the battery was embedded into the frame and the leg design was slightly modified. Although the structure was built, we were unable to test it before the due date of this paper.

VI. Conclusions and Future Work

In this paper we have collected various technologies developed for other microrobots including fabrication techniques for the stucture and actuators developed for a small robot flying insect and power electronics and control circuitry that were developed for a microglider, and applied them in the construction of our own design of a biomimetic 3g crawler. We have found that all of the technologies described in this paper could be successfully adapted to our own structure. Using these techniques along with the programming and bioinspired fiber arrays, we hope to successfully prototype an actual crawling mechanism. Future work will also include looking into reducing the technologies and techniques into a kit in which a variety of fully functional microrobots could be built.

Acknowledgment

The authors would like to thank Stan Baek, Carmel Madjidi, Mike Seeman, Aaron Hoover, Jon Entwistle, and Yohei Maeno for useful discussions.

References

[1] L. Phee, et al., “Analysis and development of locomotion devices for the gastrointestinal tract,” *IEEE Trans on Biomedical Engin.*, vol. 49, no. 6, June 2002.

[2] J. Yan, R.J Wood, S. Avadhanula, M. Sitti, and R.S. Fearing, “Towards flapping wing control for a micromechanical flying insect,” *IEEE Intl Conf on Robotics and Automation*, Seoul, Korea, May 2001.

[3] D.C. Kar, “Design of statically stable walking robot: a review,” *J. of Robotic Systems*, vol. 20, no. 11, pp. 671-686, 2003.

[4] S. Kim, A.T. Asbeck, M.R. Cutkosky, and W.R. Provancher, “SpinybotII: climbing hard walls with compliant microspines,” *12th Intl Conf on Adannced Robotics*, pp.601-606, July 2005.

[5] U. Saranli, M. Buehler, and D.E. Koditschek, ″RHex: a simple and highly mobile hexapod robot,″ *Intl J. of Robotics Research*, vol. 20, pp. 616-631, July 2001.

[6] J.M. Morrey, B. Lambrecht, A.D. Horchler, R.E. Ritzmann, and R.D. Quinn, “Highly mobile and robust small quadruped robots,” *Intl Conf on Intelligent Robots and Systems*, vol. 1, pp. 82-87, Oct. 2003.

[7] T. Ebefors, J.U. Mattsson, E. Kalvesten, and G. Stemme, “A walking silicon micro-robot,” *10th Intl Conf on Solid-State Sensors and Actuators*, Sendai, Japan, pp. 1202-1205, June 1999.

[8] S. Hollar, A. Flynn, C. Bellew, K.S.J. Pister, “Solar powered 10mg silicon robot,” *MEMS 2003*, Kyoto, Japan, Jan. 2003.

[9] L.L. Howell, *Compliant Mechanisms*, John Wiley and Sons, Inc., 2001.

[10] H.D. Eckhardt, *Kinematic Design of Machines and Mechanisms*, Mcgraw-Hill Professional, 1998.

[11] R.J. Wood, S. Avadhanula, M. Menon, and R.S. Fearing, “Microrobotics using composite materials: the micromechanical flying insect thorax,” *IEEE Int. Conf. on Robotics and Automation*, vol.2, pp. 1842-1849, Sept. 2003.

[12] R.J. Wood, E. Steltz, and R.S. Fearing, “Optimal energy density piezoelectric bending actuators,” *JSA,* vol. 119, no. 2, pp. 476-488, 2005.

[13] J. Brufau, et al., “MICRON: small autonomous robot for cell manipulation applications, “ *IEEE Intl Conf on Robotics and Automation*, pp. 856-861, 2005.

[14] E. Montane, et al., “Smart power integrated circuit for piezoceramic-based microrobot,” *ESSCIRC*, 2001.

[15] R.J. Wood, et al., “Design, fabrication and initial results of a 2g autonomous glider,” *31st Annual Conf. of the IEEE Indus. Electronics Soc.*, 2005.

[16] E. Klavins and U. Saranli, “Object oriented state machines,” *Embedded Systems Magazine*, pp. 30-42, May 2002.

[17] K. Autumn, Y. A. Liang, S. T. Hsieh, W. Zesch, W. P. Chan, T. W. Kenny, R.S. Fearing, R. J. Full, ``Adhesive force of a single gecko foot-hair,'' *Nature*, vol. 405, pp. 681-684, 2000.

[18] J. Spagna, et al., *Nature*, *unpublished* , 2005

[19] R.M. Alexander, *Principles of Animal Locomotion*, Princeton University Press, 2003.

[20] M. Sitti and R. Fearing, ``Synthetic gecko foot-hair micro/nano-structures for future wall-climbing robots,'' *IEEE Int. Conf. on Robotics and Automation*, May/Sept. 2003.

[21] C. Majidi, R. Groff, and R. Fearing, ``Clumping and packing of hair arrays manufactured by nanocasting,'' *Proc. IMECE*, Nov. 2004.